Articles

Association of DNA Quadruplexes through G:C:G:C Tetrads. Solution Structure of d(GCGGTGGAT)

Mateus Webba da Silva*

Cellular Biochemistry and Biophysics Program, Memorial Sloan-Kettering Cancer Center, 1275 York Avenue, New York, New York 10021

Received August 25, 2003; Revised Manuscript Received October 13, 2003

ABSTRACT: The structure formed by the DNA sequence d(GCGGTGGAT) in a 100 mM Na^+ solution has been determined using molecular dynamics calculations constrained by distance and dihedral restraints derived from NMR experiments performed at isotopic natural abundance. The sequence folds into a dimer of dimers. Each symmetry-related half contains two parallel stranded G:G:G:G tetrads flanked by an A:A mismatch and by four-stranded G:C:G:C tetrads. Each of the two juxtaposed G:C:G:C tetrads is composed of alternating antiparallel strands from the two halves of the dimer. For each single strand, a thymine intersperses a double chain reversal connecting the juxtaposed G:G:G:G tetrads. This architecture has potential implications in genetic recombination. It suggests a pathway for oligomerization involving association of quadruplex entities through GpC steps.

Guanine rich segments are found in biologically significant regions of the genome such as telomeres (*1*, *2*) and immunoglobin switch regions (*3*); they are observed as tandem repeats in microsatellite DNA (*4*, *5*), in sequences associated with human disease (*6*), at the replication origin of single-stranded bacteriophages and viruses (*7*, *8*), in several transcriptional regulatory regions of important oncogenes, including c-*MYC*, c-*MYB*, c-*FOS*, and c-*ABL* (*9*), and in other hot spots for genetic recombination (*10*). In solution, these segments can form three-stranded purine-(purine•pirimidine) triplex structures (*11*), as well as four-stranded quadruplex architectures (*12*−*14*) stabilized by G:G:G:G tetrads (*3*, *15*−*17*). Some evidence suggests that quadruplexes may function as transcriptional repressor elements (*18*) and that they may be involved as intermediates in recombination (*19*). Their potential role has also been suggested with the recent development of therapeutic strategies designed to stabilize telomeric ends as quadruplex structures using specific small molecules, which in turn can destabilize telomere maintenance in tumor cells (*20*−*25*).

These observations suggest that quadruplex folds in biologically functionally relevant regions could be subject to topological equilibrium: equilibrium *between* folded quadruplexes and also dynamic equilibrium with duplex as well as single-stranded DNA. In fact, interconversion between double- or single-stranded DNA and quadruplex structure in cells has been suggested to be dependent on chaperone proteins (*26*), which facilitate quadruplex formation, as well as on helicases (*27*), which are believed to resolve these structures. In general, DNA oligomerization is essential for driving formation of structural elements that are involved in a wide variety of biological processes. *In vitro*, oligomerization is known to be dependent on conditions experienced in the environment of the particular DNA sequence (*28*−*32*). *In vivo*, DNA is also prone to structural polymorphism (*33*). Biomacromolecules such as nucleic acids, proteins, and polysaccharides together with other soluble and insoluble components occupy 30−40% of the cellular volume, and their total concentration is often 400 g/L (*34*, *35*). Thus, molecular crowding should be regarded as a factor in determining the structure, stability, and function of nucleic acids (*36*−*39*), and these elements are a function of particular dynamic equilibria within biological systems.

The concept of the DNA quadruplex originated from the principle that four guanine bases can align in a plane through individual mismatch formation, involving the Watson−Crick edge of one guanine and the Hoogsteen edge of its partner around a G:G:G:G tetrad (*15*). Quadruplexes result from stacking of such tetrad (*3*, *16*, *17*) planes supported by a scaffold of four sugar−phosphate backbone columns. The tetrad repertoire was expanded to include G:C:G:C tetrads aligned through pairing of their Watson−Crick G:C base pairs along with either their major (*40*) or minor (*41*) groove edges.

Here we report on the solution structure formed by the sequence d(GCGGTGGAT) under sodium chloride conditions. The same fold fails to form in the presence of K^+ or NH_4^+. The architecture shown schematically in Figure 1a depicts an unprecedented folding topology in which two bistranded quadruplex monomeric units are linked by formation of four-stranded G:C:G:C tetrads. This topology has

* To whom correspondence should be addressed. Present address: MSRB 395, Box 2638, Research Drive, Durham, NC 27710. Phone: (919) 681-2243. Fax: (919) 668-3925. E-mail: mateus@webbas.org.

10.1021/bi0355185 CCC: $25.00
Published on Web 11/19/2003

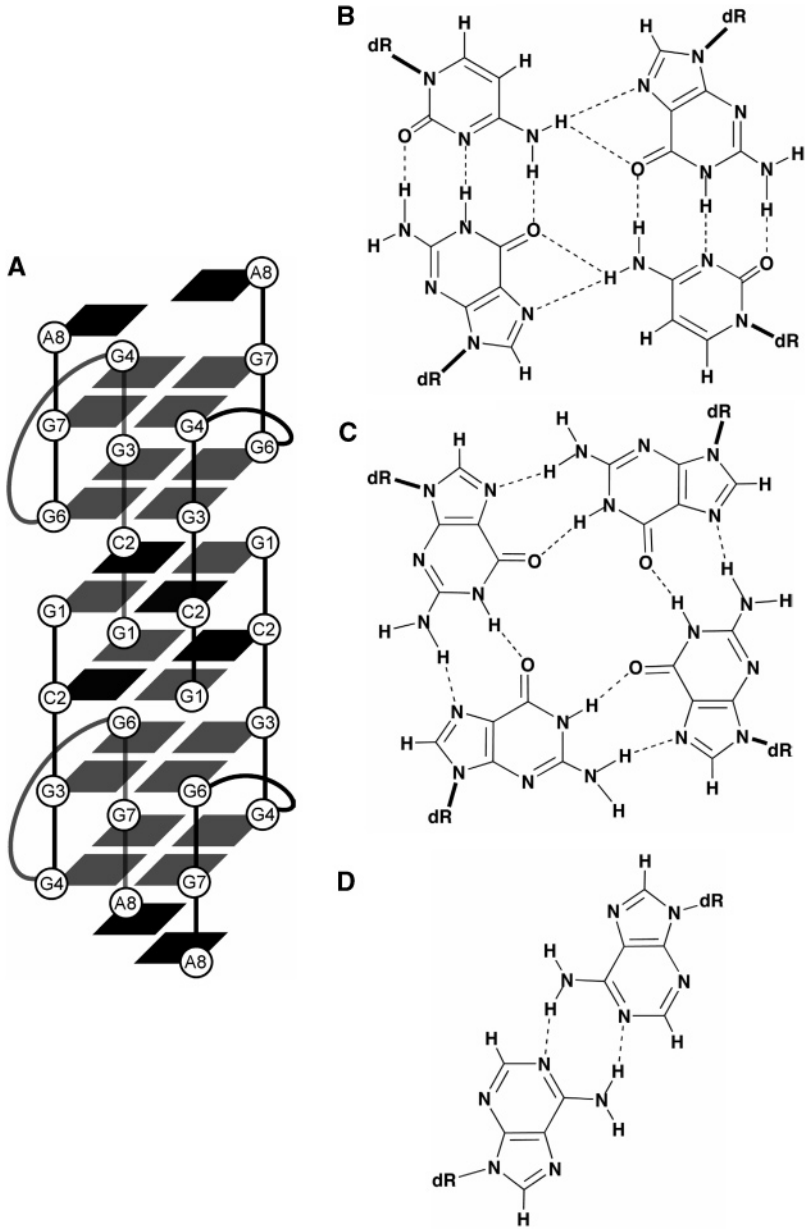

FIGURE 1: (a) Scheme of the folding topology of the four-stranded bimolecular quadruplex formed by the d(GCGGTGGAT) sequence in 0.1 M NaCl at pH 6.7. The backbone tracing of the individual strands is shown with thick lines, and non-guanine bases are depicted in black. All the guanine bases (in gray) adopt *anti* alignments. Pairing alignments for the four-stranded G1:C2:G1:C2 tetrad (b), the two-stranded G4:G7:G4:G7 tetrad (c), and the A8:A8 mismatch (d) are depicted.

potential implications in genetic recombination. Indeed, the simple architecture of this structure suggests a pathway for readily folding, and subsequently associating, quadruplex entities. For example, it can be envisaged that homologous DNA segments could be enlisted through G:C:G:C tetrad formation as a first step prior to the onset of strand exchange mediated through a pair of Holliday junction crossover sites. Furthermore, such G:C:G:C tetrad-containing quadruplex structures could also serve as potential blockage sites for the progress of GpC-containing replication forks (*42*). This study clearly shows that there are rules to be discovered that govern the folding and association of guanine rich DNA sequences.

MATERIALS AND METHODS

Synthesis and Purification of the Oligonucleotide Sequence. The nonlabeled oligonucleotide d(GCGGTGGAT) was synthesized using solid phase β-cyanoethyl phosphoramidite chemistry (see the Supporting Information). For the NMR experiments in ^2H_2O solvent, the sample was lyophilized and resuspended in 99.996% ^2H_2O. The final concentration of DNA in the sample, calculated from a UV absorbance measurement (at 260 nm), was ~6 mM (~1.5 mM per strand). The purity of the sample was assessed by NMR spectroscopy.

NMR Spectroscopy. All experiments were performed on Varian Unity *Inova* NMR 500 and 600 MHz spectrometers. Experiments were performed at a sample concentration of 3 or 6 mM. The data sets were processed using Varian software (VNMR), and the real matrices were transformed to the FELIX (Accelrys, Inc., San Diego, CA) format on Silicon Graphics (Mountain View, CA) Octane workstations. Assignments were based on homonuclear NOESY[1] (*43*), DQF-COSY (*44*), and TOCSY (*45*) and heteronuclear $^1H-^{13}C$

HSQC (*46*), $^{1}H-^{15}N$ HSQC (*47*), $^{1}H-^{31}P$ HSQC (*48*), and $^{1}H-^{13}C$ JR-HMBC (*49*) experiments. In $^{1}H_2O$, data were acquired with a jump-and-return pulse sequence (*50*) at 0 °C and in $^{2}H_2O$, with Watergate suppression of the residual water signal (*51*) at 20 °C unless otherwise stated. Data sets were acquired in a phase sensitive mode (TPPI).

Distance Restraints. A set of five NOESY mixing times (50, 100, 150, 200, and 250 ms) were used for buildup curves at 20 °C. Distances were estimated from the initial buildup rates of the NOE curves by the two-spin approximation $r_{ij} = r_{ref}(R_{ij}/R_{ref})^{1/6}$, where r_{ij} is the distance between protons i and j, r_{ref} is a reference distance, and R_{ij} and R_{ref} are the initial buildup rates. The interproton distances were estimated using the average of the volume integral of the H1′−H2″ cross-peaks as 2.20 Å of three chosen residues. Bounds were kept at ±30% and varied widely for overlapping peaks. The cross-peaks were picked manually and their volumes integrated using the FELIX (version 2.3) program. Only two limiting mixing times (60 and 200 ms) were used to derive distance restraints from the exchangeable protons collected with a jump-and-return NOESY sequence at 0 °C. Distances were thought to be 3.0 ± 0.8 Å for strong peaks, 4.0 ± 1.2 Å for medium cross-peaks observed in a 200 ms mixing time spectrum, and 5.0 ± 1.8 Å for cross-peaks not observed in a 60 ms mixing time spectrum. Atoms participating in experimentally identified canonical base pairing (based on NOE patterns) were restrained with distances corresponding to ideal hydrogen bond geometry (*52*).

Torsion Angle Restraints. Initial stereospecific assignment of individual H2′ and H2″ protons was derived from comparison of the intensity of the H1′−H2′ and H1′−H2″ intraresidue cross-peaks in a 50 ms NOESY spectrum and subsequently corroborated by analysis of a DQF-COSY spectrum. DQF-COSY spectral patterns indicated that H1′−H2″ coupling constants were reasonably large (>6 Hz) for residues G1, G3, G4, and G7, and no H2″−H3′ cross-peaks were observed for these residues. Thus, for residues G1, G3, G4, and G7, the endocyclic $\nu(0)-\nu(4)$ torsion angles were moderately constrained, leaving the sugar free to take any conformation without an energy penalty between C4′-*endo* and O1′-*endo*, including C2′-*endo*. Residues C2, T5, G6, A8, and T9 showed strong H2″−H3′ cross-peaks. Furthermore, very strong NOEs between the H6/H8 and H3′ protons (which persist at lower mixing times) independently establish an N-type preferential conformation for these residues, and therefore, loose C3′-*endo*-centered restraints were imposed on the endocyclic $\nu(0)-\nu(4)$ torsion angles. Some dihedral angles were restrained as discussed in the Results. The dihedral angle α was restrained to 0 ± 140° for G3, G4, and G7; ζ was restrained to 0 ± 140° for C2, A8, and G7, and γ was restricted to 60 ± 40° for residues G3, G4, G6, G7, and A8. The glycosidic torsion angle χ was restricted to the experimentally observed dispositions: *syn* (45 ± 90°) for residue T5 and *anti* (220 ± 70°) for all other residues.

Distance-Restrained Molecular Dynamics Regularization. Structure calculations were carried out using distance and dihedral angle constraints. Calculations were performed utilizing X-PLOR, version 3.1 (*53*), using the CHARMm force field (*54*) and adapted for restrained molecular dynamics (rMD) for nucleic acids. All calculations were executed *in vacuo* without explicit counterions. The distance geometry and simulated annealing refinement protocol started from 300 different structures generated from sets of four strands, each nine nucleotides long, randomized over all dihedral angles. A number of structures (27 of 300) emerged with the same fold and separated from nonconverged structures by large gaps in all components of the potential energy function (dihedral angles, van der Waals, NOE violations, and covalent geometry). This set was subsequently submitted to further refinement as follows.

Sets of rMD calculations were performed using random velocities fitting a Maxwell−Boltzmann distribution. The empirical energy function was developed for nucleic acids and treated all hydrogens explicitly. It consisted of energy terms for hydrogen bonding, and nonbonded interactions, bonds, bond angles, torsion angles, and tetrahedral and planar geometry, including van der Waals and electrostatic forces. The effective function included terms describing distance and dihedral restraints, which were in the form of square well potentials (*55*). Most estimated distances from NOE data analysis were incorporated as ambiguous restraints using the "SUM averaging" option of XPLOR, as they could reflect intrastrand and/or interstrand contributions. On the basis of the 4-fold symmetry, noncrystallographic symmetry restraints were imposed on all atoms. Planarity restraints were imposed throughout the computations. The final procedure consisted of a total of 53 ps of rMD, including 7 ps of 14 ps from 300 to 1000 K, a 20 ps scaleup of restraints at high temperature, 14 ps of cooling to 300 K, and 12 ps of equilibration rMD. The temperature was controlled by coupling the molecules to a temperature bath with a coupling constant of 0.025 ps (*56*). The van der Waals term was approximated using the Lennard-Jones potential energy function, and bond lengths involving hydrogens were fixed with the SHAKE algorithm (*57*) during molecular dynamics calculations. NOE and dihedral angle restraints, chemical shifts, and structure coordinates have been deposited in the Protein Data Bank (entry 1NYD).

RESULTS

The d(GCGGTGGAT) sequence forms a four-stranded quadruplex in 0.1 M NaCl with the folding topology shown schematically in Figure 1a. Experimental evidence in support of this multistranded architecture is outlined below.

Exchangeable Proton Assignments. Figure 2a shows the imino proton spectrum of d(GCGGTGGAT). In the 8.4−12.9 ppm exchangeable proton region, 12 resonances are clearly identifiable (including two isochronous at 10.4 ppm). The number of resonances in the 10.7−12.9 ppm imino proton region coincides with the number of guanines in the sequence. This suggests the formation of a structure with symmetry-related strands. The identification of guanine imino protons is corroborated by the detection of their one-bond correlations with attached imino ^{15}N, which fall in a characteristic region, 143−148.2 ppm, as shown in Figure

[1] Abbreviations: NOESY, nuclear Overhauser enhancement spectroscopy; TOCSY, total correlation spectroscopy; DQF-COSY, double-quantum filtered correlation spectroscopy; HSQC, heteronuclear single-quantum coherence; TPPI, time-proportional phase incrementation; JR-HMBC, jump-and-return heteronuclear multiple-bond correlation; WATERGATE, water suppression by gradient tailored excitation; rMD, restrained molecular dynamics.

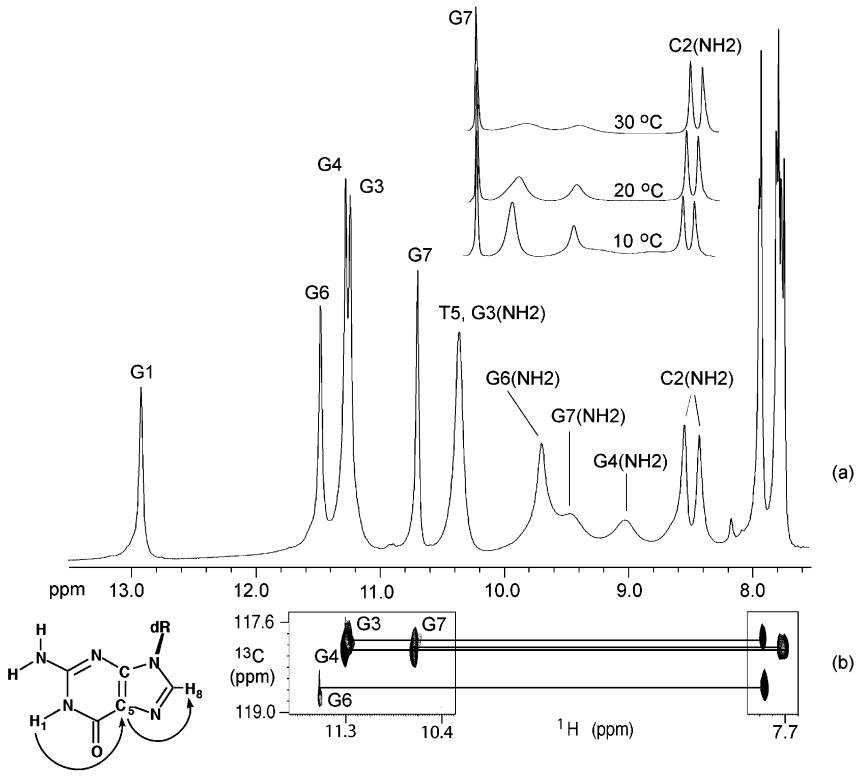

FIGURE 2: (a) Proton NMR spectrum (5.5−13.5 ppm) of d(GCGGTGGAT) in 100 mM NaCl and 2 mM phosphate in ^1H_2O at pH 6.7 and 0 °C. The assignments of the imino and amino protons are listed over the resonances. At the top, a variable-temperature plot depicts the temperature dependence between 0 and 30 °C of the hydrogen bonds securing the tetrads. (b) Aromatic H8 proton to imino proton correlation (JR-HMBC) spectrum of unlabeled d(GCGGTGGAT) in 100 mM NaCl and 2 mM phosphate in ^1H_2O at 10 °C. This intraresidue correlation allowed for the identification of the individual guanine exchangeable protons from the assigned nonexchangeable protons. The through-bond correlation path involves the large (5−9 Hz) long-range scalar couplings between ^{1}H imino═^{13}C C5 and between ^{1}H H8−^{13}C C5 pairs. The experiment was recorded with spectral widths of 14 kHz in t_2 and 0.6 kHz in t_1. A total of 3488 transients per FID with 1792 (t_2) × 40 (t_1) complex data points were acquired, resulting in the following acquisition times: $t_{2max}(^1H) = 64$ ms and $t_{1max}(^{13}C) = 30$ ms. A recycle delay of 1.5 s was used, resulting in a total experimental time of 64 h.

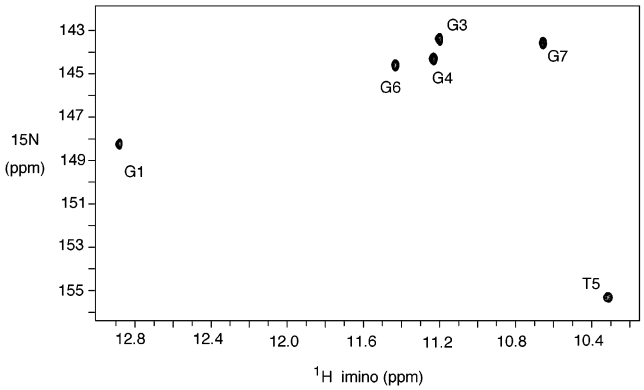

FIGURE 3: Expansion of a ^{1}H−^{15}N HSQC spectrum recorded in ^1H_2O at 0 °C. Five high-field imino-bound ^{15}N chemical shifts appear in a region characteristic of guanines, and only one signal appears in the region characteristic of thymine imino-bound ^{15}N signals. The recorded data set consisted of 1152 (t_2) and 90 (t_1) complex points with 336 transients per FID. Spectral widths of 1.2 kHz ($t_{1max} = 37.5$ ms) and 8 kHz ($t_{2max} = 72.0$ ms) were employed. The final two-dimensional matrix consisted of 2048 (w_2) × 256 (w_1) points.

3. The resonance at 155.3 ppm falls in a region characteristic of thymine ^{15}N imino resonances and is correlated to a proton at 10.4 ppm. A thymine imino proton peak in that region indicates that it is not forming hydrogen bonds in a canonical A:T base pair. The appearance of resonances in the 10.7−11.6 ppm region is characteristic of NH···N hydrogen bond alignment associated with G:G:G:G tetrad formation (*58*, *59*). The remaining guanine proton resonates in a region characteristic of NH···O═C hydrogen bond alignment characteristic of Watson−Crick G:C base pair formation associated with G:C:G:C tetrad formation.

Analysis of a long-range coupling ^{1}H−^{13}C JRHMBC experiment (*49*) allowed the assignment of the exchangeable imino protons from the assigned nonexchangeable H8 protons of individual guanine residues (see below) (Figure 2c). Guanine imino protons were correlated with their nonexchageable H8 through intraresidue heteronuclear couplings $^3J_{H1-C5}$ (5−9 Hz) and $^3J_{H8-C5}$ (∼10 Hz) under natural isotopic abundance. Assignments of amino protons (Figure 2a) were obtained from their strong NOE connectivities to imino protons.

Nonexchangeable Proton Assignments. The nonexchangeable ^{1}H, ^{13}C, ^{15}N, and ^{31}P resonances of d(GCGGTGGAT) were assigned using standard methods (*47*, *60*). Sequential assignments were made on the basis of the H6/H8−H1′ connectivities and proceeded through analysis of the 50 and 250 ms NOESY spectra. These were further substantiated by sequential analysis of H6/H8−H3′ connectivity, by aromatic−aromatic cross-peaks, and by H6/H8−H2′/H2″ connectivities. In a plot of a NOESY spectrum collected with a mixing time of 250 ms, we can trace the sequential connectivities between the base and its own and 5′-flanking sugar H1′ protons along individual strands (Figure 4a). Except for residue T5, weak intraresidue H8/H6−H1′ cross-peaks were observed, indicating that residues are *anti*. The

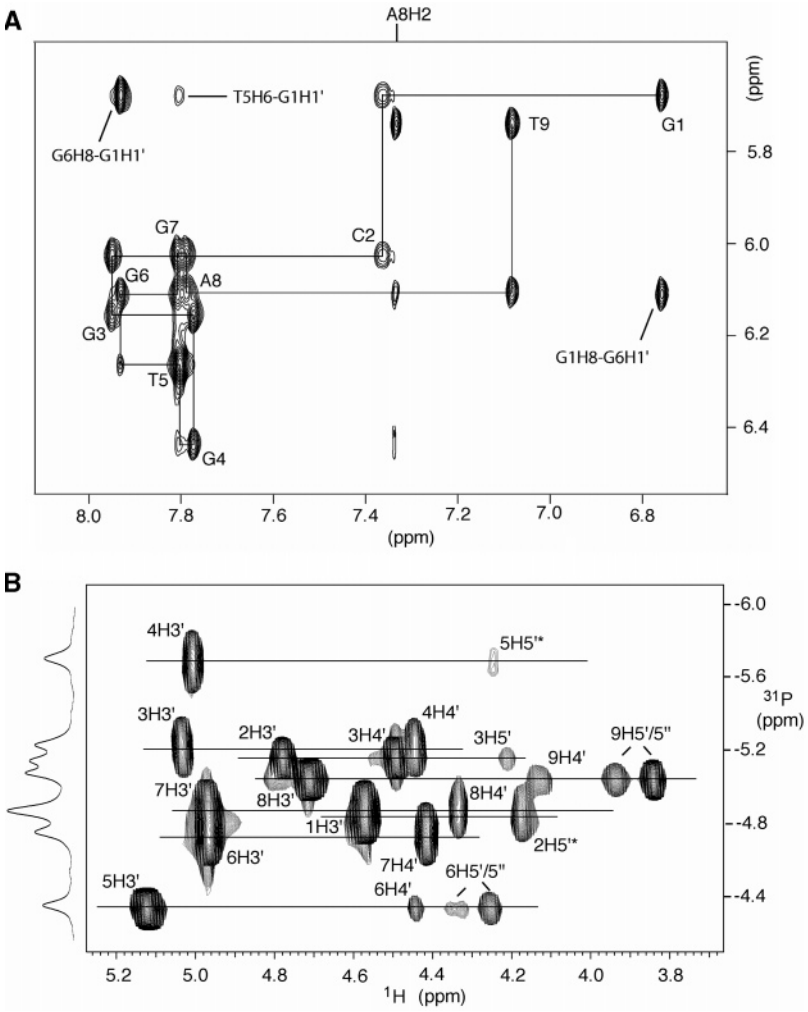

FIGURE 4: (a) Expanded NOESY (mixing time of 250 ms) spectrum recorded in ^2H_2O at 20 °C correlating the aromatic base proton and sugar H1′ for d[(GCGGTGGAT)$_2$]$_2$. The lines trace the NOE connectivities between the base protons and their own and 5′-flanking sugar H1′ protons from G1 to T9 in the sequence. Both G1 H8−G6 H1′ and G6 H1′−G1 H8 cross-peaks are crucial assignments leading to the identification of the architecture of the quadruplex formed by the d(GCGGTGGAT) sequence in a Na^+ salt solution. (b) $^{31}P-^1H$ correlation spectrum of d(GCGGTGGAT) in 100 mM NaCl (pH 6.7) at 20 °C.

T5 H6−T5 H1′ cross-peak was comparably stronger, indicating the *syn* nature of its glycosidic torsion angle χ. The initial assignment of A8 H2 was derived from the typical intraresidue A8 H1′−A8 H2 and T9 H1′−A8 H2 connectivities. Corroboration of assignments of ^{1}H resonances followed analysis of the characteristic chemical shifts of attached ^{13}C. Further evidence for sugar H3′ and some H4′/H5′/H5″ was gathered through analysis of their magnetization transfers to backbone ^{31}P (Figure 4b). The latter are also sequential in nature: H3′(i − 1)−P(i − 1)−H4′/H5′/H5″(i). The ^{31}P chemical shifts were used to exclude the *trans* domain for both ζ (C3′−O3′−P−O5′) and α (O3′−P−O5′−C5′) torsion angles (*61*), since ^{31}P signals resonate in the normal 1 ppm range; then both the ζ and α backbone angles are not in the *trans* domain. Thus, the α dihedrals for G3, G4, and G7 were restrained to 0 ± 140°. These are all C2′-*endo* sugar puckers. G6 was excluded because of its very downfield ^{31}P shift, for which major distortion is expected. The dihedral angle ζ was restricted only for the least distorted of the residues. Thus, residues within 0.3 ppm of "free" phosphate (P9) were also restricted to 0 ± 140°: C2, A8, and G7. Since the ability to detect $^4J_{H4'-P}$ couplings indicates that in B-helix DNA γ torsion angles are in the *gauche*$^+$ domain (*62*), the dihedral angle γ was restrained to 60 ± 40° for residues G3, G4, G6, G7, and A8. A total of 11 dihedral angles were used for rMD calculations.

Identification of the Topology. Figure 1b−d depicts the hydrogen bonding alignments that make up the global architecture. A pattern of NOEs characteristic of G:G:G:G tetrad formation is observed in the JR-NOESY (mixing time of 200 ms) data set (Figure 5). Both amino and imino protons of G6 show cross-peaks to H8 of G3 (peaks d and q). This pattern is characteristic of G3:G6:G3:G6 tetrad formation and defines the directionality of guanine Watson−Crick edge to Hoogsteen edge alignments for the tetrad. Unfortunately, the amino protons of G7 and G4 cannot be observed (Figure 2a), possibly because of a more solvent exposed tetrad. However, there are NOEs between the imino protons of G4 and H8 of G7 (peak g), and also between the imino protons of G7 and H8 of G4 (peak l). These along with other cross-peaks were sufficient to characterize G4:G7:G4:G7 tetrad formation. Another set of NOEs defines the relative donor−acceptor hydrogen bond directionalities for the G1:C2:G1:C2 tetrad. NOEs between H8 of G1 and both C2 H5 (peak not shown) and the amino group of C2 (peak s), as well as the imino group of G1 and the amino group of

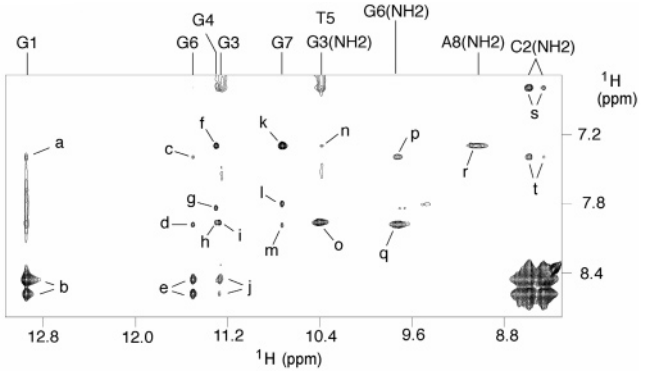

FIGURE 5: Expanded JR-NOESY spectrum (60 ms) of d(GCGGTGGAT) in 100 mM NaCl and 2 mM sodium phosphate buffer at pH 6.6 in ^1H_2O at 0 °C, exhibiting dipolar connectivities between imino and aromatic protons. Peaks a−t are assigned as follows: (a) G1 NH1−C2 H6, (b) G1 NH1−C2 NH_2, (c) G6 NH1−C2 H6, (d) G6 NH1−G3 H8, (e) G6 NH1−C2 NH_2, (f) G4 NH1−A8 H2, (g) G4 NH1−G7 H8, (h) G4 NH1−G6 H8, (i) G3 NH1−G6 H8, (j) G3 NH1−C2 NH_2, (k) G7 NH1−A8 H2, (l) G7 NH1−G4 H8, (m) G7 NH1−G3 H8, (n) G3 NH_2−A8 H2, (o) G3 NH_2−G6 H8, (p) G6 NH_2−C2 H6, (q) G6 NH_2−G3 H8, (r) A8 NH_2−A8 H2, (s) C2 NH_2−G1 H8, and (t) C2 NH_2−C2 H6.

C2 (peak b), were detected. These observations verify the direct alignment of opposing Watson−Crick G1:C2 pairs through their major groove edges. Assignment of the A8:A8 mismatch is supported by a number of connectivities, including the A8 NH_2−A8 H2 cross-peak (peak r) observed both at 200 ms and at 60 ms. This is only possible if the cross-peak is an interresidue one with an H-bonding alignment as in Figure 1d. Concomitantly, only one of the amino protons is hydrogen bound as suggested by their difference in chemical shifts [$\Delta\delta$ = 2.3 ppm (not shown)]. Further connectivities were instrumental in describing the disposition of the adenines. Essentially, the identification of G1:C2:G1:C2, G3:G6:G3:G6, and G4:G7:G4:G7 tetrads establishes that the d(GCGGTGGAT) sequence forms a quadruplex.

Inspection of Figure 1a suggests that nonsequential connectivities could be instrumental in establishing the global fold. In this context, some NOEs were found to reflect aspects of the stacking between structured elements in the architecture of the quadruplex. Among others, dipolar G6 H8−G1 H1′, G1 H8−G6 H1′ (both shown in Figure 2a), G1 H8−G6 H8, G6 H8−C2 H6, and G1 H1−G6 H1 (not shown) connectivities place G6 juxtaposed with G1 (Figure 1a). Dipolar G6 H1−C2 NH2 and G3 H1−C2 NH2 connectivities (peaks e and j, respectively, in Figure 5) justify juxtaposition of G1:C2:G1:C2 and G3:G6:G3:G6 tetrads. Cross-peaks between the imino protons of guanines indicate stacking involving G3:G6:G3:G6 and G4:G7:G4:G7 tetrads (not shown). G4 NH1−A8 H2 (f), G7 NH1−A8 H2 (l) cross-peaks and in Figure 2a the long-range A8 H2−G4 H1′ cross-peak place this adenine stacking with the G4:G7:G4:G7 tetrad. Juxtaposition of the adenine mismatch with the G4:G7:G4:G7 tetrad, with G4:G7:G4:G7 and G3:G6:G3:G6 tetrads, and with G3:G6:G3:G6 and G1:C2:G1:C2 tetrads indicates the sequential disposition of the planar structured elements within the quadruplex. The T5 H6−G1 H1′ cross-peak in Figure 2a, along with other connectivities involving the methyl group of thymine T5 and sugar protons of G1 and C2 (not shown, T5 Me−G1 H1′, T5 Me−G1 H4′, T5 Me−C2 H1′, and T5 Me−C2 H2″), indicates that the Watson−Crick edge for this residue points away from the quadruplex. Furthermore, these contacts place this thymine close to the G1:C2:G1:C2 tetrad.

Table 1: NMR Restraints and Structural Statistics for 10 Selected Structures for the Dimeric d(GCGGTGGAT) Quadruplex

no. of NMR restraints	
total	256
nonexchangeable protons[a]	136
exchangeable protons[a]	36
hydrogen bond restraints (empirical)[a]	28
deoxyribose pseudorotation restraints	36
phosphodiester torsion angle restraints[b]	11
glycosidic torsion angle restraints[b]	9
noncrystallographic symmetry restraints on all heavy atoms	
structural statistics	
NOE rmsd (Å), total	0.034 ± 0.005
NOE violations exceeding 0.2 Å	0
rmsds from ideal covalent geometry	
bond lengths (Å)	0.0083 ± 0.0004
bond angles (deg)	3.1 ± 0.2
impropers (deg)	0.43 ± 0.02
pairwise rmsd for all heavy atoms (Å)	0.4 ± 0.1

[a] Distance restraints per strand. [b] Number of restraints per strand.

Structural Features. After molecular dynamics regularization, a set of 10 structures exhibiting pairwise heavy atom root-mean-square deviation (rmsd) values of 0.41 ± 0.1 was selected on the basis of the lowest overall energy. The global structure of the quadruplex formed by the d(GCGGTGGAT) sequence under moderate salt conditions and pH 6.7 (100 mM NaCl and sodium phosphate buffer) consists therefore of homomultimeric association that results in a bimolecular topology. A stereoview of the selected 10 superpositioned refined structures is given in Figure 6a. The input and structure convergence parameters are listed in Table 1.

The right-handed tetrameric quadruplex consists of antiparallel strands at its four-stranded core, and parallel strands as part of its two bistranded regions. In the interface of the dimer, two four-stranded G1:C2:G1:C2 tetrads stack. G:C:G:C tetrad formation involves hydrogen bonding alignment of two Watson−Crick G:C base pairs through their major groove edges (*63*) using bifurcated hydrogen bonds. Both amino protons of the cytidine residues are hydrogen bound within the G:C:G:C tetrads. End-to-end stacking of these tetrads constitutes the 5′−5′ interface of the dimer of dimers. The internal G1:C2:G1:C2 tetrads are flanked by G3:G6:G3:G6 tetrads. These tetrads are part of bistranded regions of the topology, featuring juxtaposed G6:G3:G6:G3 and G4:G7:G4:G7 tetrads. Hydrogen bond alignment through Watson−Crick and Hoogsteen edges of these guanines in parallel strands results in G(*anti*):G(*anti*):G(*anti*):G(*anti*) alignments. The polarity of the strands results from a double chain reversal that involves both of these G:G:G:G tetrads. The thymine (T5) is bracketed by tetrad-forming guanines in the G3pG4T5G6pG7 segment. Nonstandard backbone torsion angles are observed for residues participating in the chain reversals (see Table S1 of the Supporting Information). Dihedral angle values are in the *gauche*$^+$ range for β in T5 and ζ in G6. The *gauche*$^-$ region is preferential for ϵ in T5 and β in both G6 and G7. Typical values for β and ϵ in B-, A-, and Z-DNA are in the *trans* range, with the exception of ϵ for which Z-DNA is characteristically *gauche*$^-$. For G6,

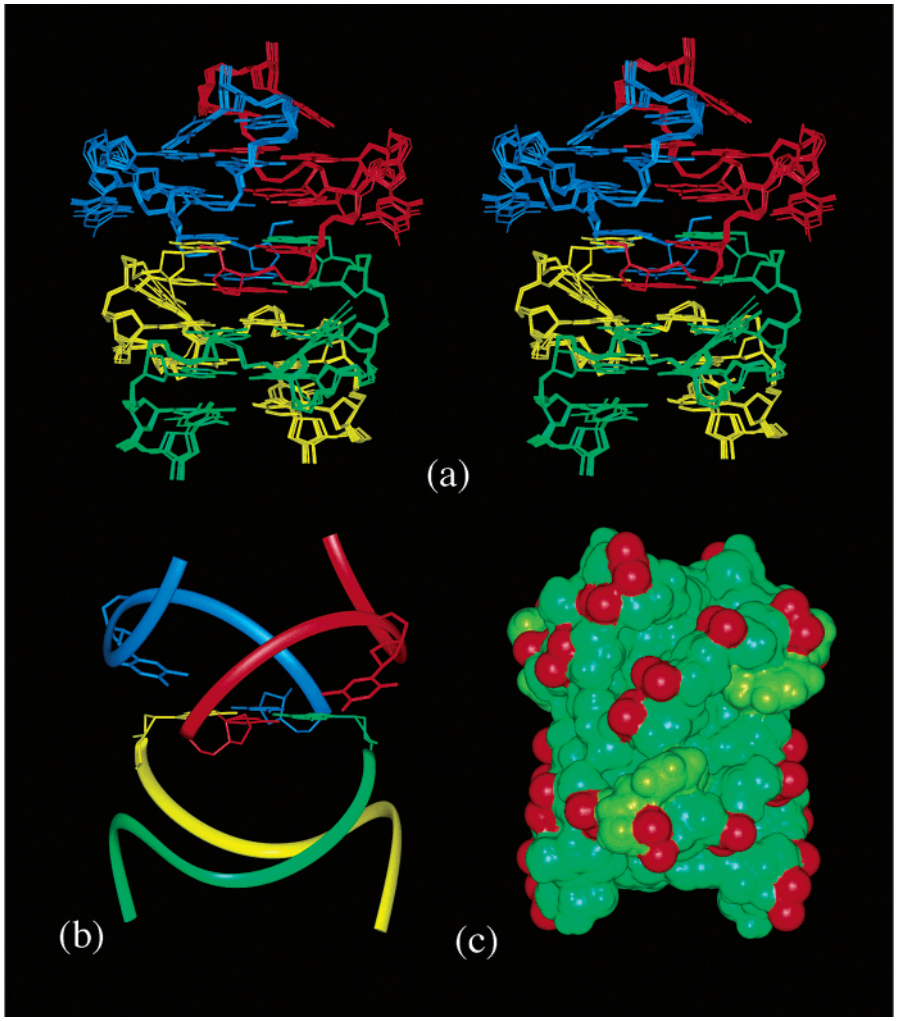

FIGURE 6: (a) Stereoview of a superposition of 10 refined structures of the quadruplex formed by the d(GCGGTGGAT) sequence in a sodium solution. The individual strands are colored yellow, cyan, green, and red. Protons and the exocyclic phosphate oxygens have been omitted for clarity. (b) Stick depiction of the backbone of the lowest-energy refined structure of the quadruplex motif. The looping thymine points its methyl to a G:C:G:C tetrad. (c) Space filling view of a the lowest-energy refined structure. The looping thymine is depicted in lighter green, and the backbone phosphorus atoms are colored red.

the torsion angle ϵ is preferentially *gauche*$^-$, α is *trans*, and the range of ζ (*gauche*$^+$) is characteristic of Z-DNA. Notable backbone features are also the dihedral angles α,*t* and β,g^- for C2 and ϵ,g^- for A8. They reflect the extent of backbone distortions necessary to accommodate the dimer interface G:C:G:C tetrad and the capping A:A mismatch, respectively.

There is apparent order in the context of the position of the chemical shift of ^{31}P in view of the double chain reversal defined by residues G3−G7 (Figure 3b). Thymine T9 is a terminal residue that is not base-paired. Its phosphorus, P9, should be one of the least strained phosphates, and thus, it appears close to the center of the spectral width covered by the ^{31}P chemical shifts. Phosphorus chemical shifts for the G3pG4pT5 fragment appear downfield to P9, and those for the G6pG7 fragment are upfield. Furthermore, the closer the phosphates in the backbone are to residues in the chain reversal T5 and G6, the more dramatic the downfield or upfield shift. This conformational coupling is mediated by the shared furanose rings at the step junctions. The two distinct regions, G3pG4 and G6pG7, are bracketed by residues with sugar puckers populating preferentially C3′-*endo* sugar puckers: C2, T5, and A8. Therefore, the sequential interdigitation of C2′-*endo* and C3′-*endo* puckering illustrates the accommodation of trends in the collective mechanics in the DNA backbone that result from the double chain reversal.

The stacking overlap between the A8:A8 mismatch and the G7:G4:G7:G4 tetrad is shown in Figure 7a. Purines G7 and A8 in the G7pA8 step stack extensively (while pyrimidine T9 is not coplanar with either the A8:A8 mismatch or the G7:G4:G7:G4 tetrad, not shown). The good stacking pattern for G7:G4:G7:G4 and G6:G3:G6:G3 tetrads is shown in Figure 7b. There is close to maximum overlap between the purine rings within individual GpG steps. The hydrogen bond directionalities from Watson−Crick to Hoogsteen edges point in the same direction (Figure 7b). Good stacking is also observed between G6:G3:G6:G3 and G1:C2:G1:C2 tetrads (Figure 7c), even though the hydrogen bond directionalities point in opposite directions. Good stacking is also observed for G3 and G1 of different strands, and for G6 and C2 of the same strand. The stacking overlap pattern between symmetry-related G:C:G:C tetrads across the dimeric interface is shown in Figure 7d. The Watson−Crick and major groove edge-aligned G:C:G:C tetrads point in opposite

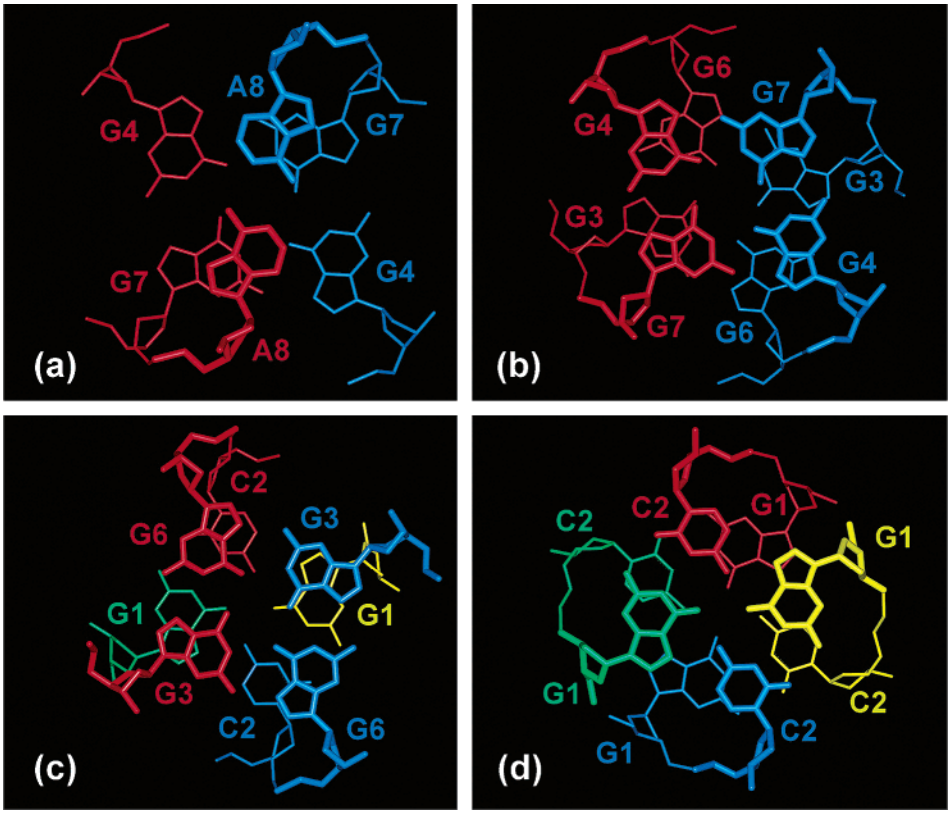

FIGURE 7: Stacking overlap patterns between nearest-neighbor planar elements in the lowest-energy refined structure of the four-stranded d(GCGGTGGAT) quadruplex formed in a sodium solution. Overlap geometry (a) between the A8:A8 mismatch and G4:G7:G4:G7 tetrad, (b) between G4:G7:G4:G7 and G3:G6:G3:G6 tetrads, (c) between G3:G6:G3:G6 and G1:C2:G1:C2 tetrads, and (d) between adjacent G1:C2:G1:C2 tetrads. All hydrogen atoms and phosphate oxygen atoms in the backbone have been omitted for clarity.

directions (Figure 7d) for these adjacent tetrad motifs. The stacking patterns reflect overwound G1pC2 steps that result in a measure of interstrand stacking.

DISCUSSION

Double repeats of guanines interspersed by two or more bases have the tendency to fold into dimeric structures (*64*). In a 100 mM sodium solution, the d(GCGGTGGAT) sequence forms a 4-fold symmetric bimolecular quadruplex in which two strands of each monomer associate in a stacked array comprised of a reversed A:A mismatch, and two adjacent G:G:G:G tetrads. The association of two bistranded units through 5′-GpC ends results in the formation of two juxtaposed four-stranded G:C:G:C tetrads. The tetrads in both quadruplexes have the characteristic square planar arrangement found in simple quadruplexes, with base pairing through their Watson−Crick and Hoogsteen edges. Four continuous grooves with the same width span the quadruplex architecture. Figure 6c depicts a Connoly view of the global molecule with the phosphates in red and showing hydrophobic clefts running from end to end across the molecule. Two of these are occupied by a pair of looping thymines (Figure 6b). Apparently, their presence, or absence, does not induce groove width variations. These thymines intersperse a double chain reversal connecting the top of one strand with the bottom of the other of the juxtaposed G:G:G:G tetrads. The resultant arrangement ensures the integrity of the tetrads, strand parallelism, and the same groove width within the moiety of the G:G:G:G tetrads. Shallow turns occur in the backbone for the G3−T5 segment and G6pG7 step. Bracketing the double chain reversal are C3′-*endo* sugar puckers for C2 and A8. This feature illustrates the extent of the accommodation of sugar pucker torsions to the backbone in the double chain reversal. The stem oligonucleotides are all in an *anti* conformation, while the looping thymines are *syn*. The latter may be a consequence of the effort to optimize the hydrophobic interactions partially resultant from the methyl group of the looping thymine, and reflects the preferential glycosidic torsion angle adopted by nonbonded thymines. This is apparent from assessing the water accessibility to the amino protons of the guanines. Depicted in Figure 2a are spectra of the exchangeable proton signals in the temperature range of 0−30 °C. At 30 °C, the amino protons for G3 and G6 can still be observed, while those for G4 and G7 cannot. This indicates that solvent accessibility at the G3:G6:G3:G6 tetrad seems to be reasonably impaired as compared to the top tetrad, G4:G7:G4:G7, therefore suggesting the increased hydrophobic character. *In suma*, the backbone of the four symmetry-related strands assumes an S-shaped configuration and the dimer adopts a compact fold in which both thymines in the nonamer are not base paired. The A8:A8 mismatch serves a capping function, helping to maintain this compact fold. Contributing to the stabilization of this compact topology is the presence of Na^+ ions. Ions such as K^+ and NH_4^+ did not promote the same fold at concentrations of 10−400 mM. Attempts were made from a freshly prepared sample using these ions. Presumably, they are too large either to coordinate in the plane of the G:G:G:G tetrads, to stabilize the one-residue loops, or both. Increasing or decreasing the sodium salt concentration (15−400 mM) did not promote recognition of the sheared edge of either the G6:G3:G6:G3 or G7:G4:G7:G4 tetrad by the

looping thymine probably because of the preferential *syn* glycosidic angle that nonbound thymines preferentially adopt.

Comparisons to Known Structures. The identification of the double chain reversal loops (*65*) introduced a novel concept for bridging adjacent parallel aligned G_n segments within a quadruplex. This feature has been recently observed in the structure of quadruplexes adopted by human telomeric repeats (*66*). Both d(TAGGGTTAGGGT) and d[AGGG-$(TTAGGG)_3$] sequences form quadruplexes that exhibit 4-fold noncrystallographic pseudosymmetry. In both structures, three residues (TTA) are the looping appendages. The example of double chain reversal presented here was first reported within the folding topology of the unimolecular quadruplex formed by the *Tetrahymena* $d(TTGGGG)_4$ telomeric sequence and involved the GGTTGG segment (*65*). In all these telomeric sequences, the thymines loop out and do not recognize the sheared edge of the guanines in the quadruplex. Their positioning in a quadruplex groove serves a steric blockage function for recognition of the sheared edge of the guanine part of the tetrads. They also provide a recognition function since the Watson−Crick edge for all looping residues is thus available for recognition. Loops may thus serve as attractive targets for small molecules and other nucleic acid segments. This concept is recognized from the fact that thrombin is known to target the loop segments rather than the quadruplex scaffold of the thrombin binding DNA aptamer (*67*). It is consequently apparent that selective targeting of loops in quadruplex folds will benefit from a better understanding of the diversity and knowledge of structural details of such higher-order architectures.

Interestingly, a T:T:T:T tetrad was identified in the $[d(TGGTGGC)]_4$ sequence, where the tetrad-forming thymines are trapped between two G:G:G:G tetrads (*68*). The thymines associate via an NH3···O4 hydrogen bond that protects the thymine imino proton from exchange with bulk water. Notably, in this sequence, the GGTGG segment does not lead to formation of loops. This may be due to the fact that the structure was identified in a K^+ salt solution.

Segments in which A ≡ N in GGNGG are known to fold into quadruplexes (*32*, *69*, *70*) and are similar in some ways to the architecture of the $[d(GCGGTGGAT)_2]_2$ sequence. Guanines in the GGAGG segment are generally found as part of tetrads in parallel strands. The parallel alignment of the GpG segments is the result of two successive turns interspersed with the Hoogsteen edge-bound adenines that recognize the sheared edge of the tetrad-forming guanines, thus ensuring formation of a G(A-G) triad. In the discovery of this motif, Kettani et al. (*71*) found that at high salt concentrations (150 mM sodium) the $[d(GGAGGAG)]_2$ sequence forms a dimeric structure in which each monomer associates in a stacked array of a reversed A:A mismatch, a G:G:G:G tetrad, and a A(G:G:G:G)A hexad. In contrast to the $[d(GCGGTGGAT)_2]_2$ sequence, a sharp turn in the backbone occurs at G2 (that is stabilized by formation of the triad) and a shallower turn occurs at the A3pG4 step. The extensive stacking between two such monomers accounts for the stability of the dimer at moderate to high concentrations. At low sodium salt concentrations, the sequence converts to a duplex arrowhead motif (*72*).

Biological Significance. Ion-induced conformational changes are the basis of the postulate that DNA quadruplexes may function as molecular switches (*73*, *74*). Thus, formation of the present architecture in Na^+, but not in K^+, suggests possible relevance in DNA signaling mechanisms. The homomultimeric bimolecular dimer formed by the d(GCG-GTGGAT) nonamer suggests that quadruplexes can undergo further oligomerization without rearrangement of their quadruplex fold. The simple architecture of this structure suggests a pathway for readily folding, and subsequently associating, quadruplex entities. It suggests that it is possible to stabilize, even transiently, GpC dangling ends of quadruplex monomeric entities as G:C:G:C tetrads. This mechanism might account for the blockage of the fragile X locus observed experimentally (*75*), since the phase of the $d(CGG)_n$ fragile X syndrome triplet repeat can be either CGG, GGC, or GCG. The hypothesis that quadruplex types of structures are intermediates in recombination would suggest the possibility of such facile folding and quadruplex entity interaction. This is also of consequence in the design and engineering of folds comprised of short sequences containing CpG dinucleotides in appropriate sequential contexts for specific delivery to particular biological targets (*76*−*78*).

It therefore would appear to be crucial that an understanding of specific motif stabilization at the molecular level requires reasonably detailed structures in a variety of contexts. Structural studies of this type are fundamental for an understanding of the possible topologies, recognition elements, and concerted structural mechanics that are at the basis of DNA polymorphism and association, with relevance in a varied array of functions in biological systems.

ACKNOWLEDGMENT

Anh-Tuan Phan is gratefully acknowledged for useful discussions.

SUPPORTING INFORMATION AVAILABLE

Synthesis and purification of the oligonucleotide sequence and torsion angles for the lowest-energy structure of the $[(GCGGTGGAT)_2]_2$ sequence. This material is available free of charge via the Internet at http://pubs.acs.org.

REFERENCES

1. Blackburn, E. H., and Szostak, J. W. (1984) *Annu. Rev. Biochem. 53*, 163−194.
2. Blackburn, E. H. (1994) *Cell 77*, 621−623.
3. Sen, D., and Gilbert, W. (1988) *Nature 334*, 364−366.
4. Birnboim, H. C., Sederoff, R. R., and Paterson, M. C. (1979) *Eur. J. Biochem. 98*, 301−307.
5. Lohe, A. R., Hilliker, A. J., and Roberts, P. A. (1993) *Genetics 134*, 1149−1174.
6. Fry, M., and Loeb, L. A. (1994) *Proc. Natl. Acad. Sci. U.S.A. 91*, 4950−4954.
7. Grosschedl, R., and Hobom, G. (1979) *Nature 277*, 621−627.
8. Hirao, I., Nishimura, Y., Naraoka, T., Watanabe, K., Arata, Y., and Miura, K. (1989) *Nucleic Acids Res. 17*, 2223−2231.
9. Simonsson, T., Pecinka, P., and Kubista, M. (1998) *Nucleic Acids Res. 26*, 1167−1172.
10. Wells, R. D., Collier, D. A., Hanvey, J. C., Shimizu, M., and Wohlrab, F. (1988) *FASEB J. 2*, 2939−2949.
11. Wang, E., and Feigon, J. (1999) in *Oxford Handbook of Nucleic Acid Structures* (Neidle, S., Ed.) pp 355−388, Oxford University Press, Oxford, U.K.
12. Williamson, J. R. (1994) *Annu. Rev. Biophys. Biomol. Struct. 23*, 703−730.
13. Rhodes, D., and Giraldo, R. (1995) *Curr. Opin. Struct. Biol. 5*, 311−322.

14. Patel, D. J., Bouaziz, S., Kettani, A., and Wang, Y. (1999) in *Oxford Handbook of Nucleic Acid Structures* (Neidle, S., Ed.) pp 389−453, Oxford University Press, Oxford, U.K.
15. Gellert, M., Lipsett, M. N., and Davies, D. R. (1962) *Proc. Natl. Acad. Sci. U.S.A. 48*, 2013−2018.
16. Sundquist, W. I., and Klug, A. (1989) *Nature 342*, 825−829.
17. Williamson, J. R., Raghuraman, M. K., and Cech, T. R. (1989) *Cell 59*, 871−880.
18. Siddiqui-Jain, A., Grand, C. L., Bearss, D. J., and Hurley, L. H. (2002) *Proc. Natl. Acad. Sci. U.S.A. 99*, 11593−11598.
19. Sun, H., Yabuki, A., and Maizels, N. (2001) *Proc. Natl. Acad. Sci. U.S.A. 98*, 12444−12449.
20. Mergny, J. L., and Helene, C. (1998) *Nat. Med. 4*, 1366−1367.
21. Bearss, D. J., Hurley, L. H., and Von Hoff, D. D. (2000) *Oncogene 19*, 6632−6641.
22. Gowan, S. M., Harrison, J. R., Patterson, L., Valenti, M., Read, M. A., Neidle, S., and Kelland, L. R. (2002) *Mol. Pharmacol. 61*, 1154−1162.
23. Read, M., Harrison, R. J., Romagnoli, B., Tanious, F. A., Gowan, S. H., Reszka, A. P., Wilson, W. D., Kelland, L. R., and Neidle, S. (2001) *Proc. Natl. Acad. Sci. U.S.A. 98*, 4844−4849.
24. Mergny, J. L., Lacroix, L., Teulade-Fichou, M. P., Hounsou, C., Guittat, L., Hoarau, M., Arimondo, P. B., Vigneron, J. P., Lehn, J. M., Riou, J. F., Garestier, T., and Helene, C. (2001) *Proc. Natl. Acad. Sci. U.S.A. 98*, 3062−3067.
25. Mergny, J. L., and Maurizot, J. C. (2001) *ChemBioChem 2*, 124−132.
26. Fang, G. C., Cheh, T. R. (1993) *Cell 74*, 875−885.
27. Sun, H., Bennett, R. J., and Maizels, N. (1999) *Nucleic Acids Res. 27*, 1978−1984.
28. Miyoshi, D., Nakao, A., and Sugimoto, N. (2002) *Biochemistry 41*, 15017−15024.
29. Miyoshi, D., Nakao, A., and Sugimoto, N. (2003) *Nucleic Acids Res. 31*, 1156−1163.
30. Crnugelj, M., Hud, N. V., and Plavec, J. (2002) *J. Mol. Biol. 320*, 911−924.
31. Bouaziz, S., Kettani, A., and Patel, D. J. (1998) *J. Mol. Biol. 282*, 637−652.
32. Kettani, A., Gorin, A., Majumdar, A., Hermann, T., Skripkin, E., Zhao, H., Jones, R., and Patel, D. J. (2000) *J. Mol. Biol. 297*, 627−644.
33. Rich, A. (1993) *Gene 135*, 99−109.
34. Minton, A. P. (2001) *J. Biol. Chem. 276*, 10577−10580.
35. Ellis, R. J. (2001) *Curr. Opin. Struct. Biol. 11*, 114−119.
36. Minton, A. P. (2000) *Curr. Opin. Struct. Biol. 10*, 34−39.
37. Flaugh, S. L., and Lumb, K. J. (2001) *Biomacromolecules 2*, 538−540.
38. Hatters, D. M., Minton, A. P., and Howlett, G. J. (2002) *J. Biol. Chem. 277*, 7824−7830.
39. Martin, J. (2002) *Biochemistry 41*, 5050−5055.
40. Kettani, A., Kumar, R. A., and Patel, D. J. (1995) *J. Mol. Biol. 254*, 638−656.
41. Leonard, G. A., Zhang, S., Peterson, M. R., Harrop, S. J., Helliwell, J. R., Cruse, W. B., d'Estaintot, B. L., Kennard, O., Brown, T., and Hunter, W. N. (1995) *Structure 3*, 335−340.
42. Hansen, R., Gartler, S., Scott, C., Chen, S., and Laird, C. (1992) *Hum. Mol. Genet. 1*, 571−578.
43. Jeener, J., Meier, B. H., Bachmann, P., and Ernst, R. R. (1979) *J. Chem. Phys. 71*, 4546−4553.
44. Piantini, U., Sorensen, O. W., and Ernst, R. R. (1982) *J. Am. Chem. Soc. 104*, 6800−6801.
45. Braunschweiler, L., and Ernst, R. R. (1983) *J. Magn. Reson. 53*, 521−528.
46. Bodenhausen, G., and Ruben, D. J. (1980) *Chem. Phys. Lett. 69*, 185−188.
47. Varani, G., Abouela, F., and Allain, F. H. T. (1996) *Prog. Nucl. Magn. Reson. Spectrosc. 29*, 51−127.
48. Sklenar, V., Miyashiro, H., Zon, G., Miles, H. T., and Bax, A. (1986) *FEBS Lett. 208*, 94−98.
49. Phan, A. T. (2000) *J. Biomol. NMR 16*, 175−178.
50. Gueron, M., and Plateau, P. (1982) *J. Am. Chem. Soc. 104*, 7310−7311.
51. Piotto, M., Saudek, V., and Sklenar, V. (1992) *J. Biomol. NMR 2*, 661−665.
52. Saenger, W. (1984) *Principles of Nucleic Acid Structure*, Springer-Verlag, New York.
53. Brunger, A. T. (1992) *X-PLOR*, version 3.1, Department of Molecular Biophysics and Biochemistry, Yale University, New Haven, CT.
54. Brooks, B. R., Bruccoleri, R. E., Olafson, B. D., States, D. J., Swaminathan, S., and Karplus, M. (1983) *J. Comput. Chem. 4*, 187−217.
55. Clore, G. M., Gronenborn, A. M., Carlson, G., and Meyer, E. F. (1986) *J. Mol. Biol. 190*, 259−267.
56. Berendsen, H. J. C., Postma, J. P. M., Vangunsteren, W. F., Dinola, A., and Haak, J. R. (1984) *J. Chem. Phys. 81*, 3684−3690.
57. Ryckaert, J.-P. P. C., and Berendsen, H. J. C. (1977) *J. Comput. Phys. 23*, 327−341.
58. Smith, F. W., and Feigon, J. (1992) *Nature 356*, 164−168.
59. Wang, Y., and Patel, D. J. (1993) *Structure 1*, 263−282.
60. Wütrich, K. (1986) *NMR of Proteins and Nucleic Acids*, John Wiley & Sons, New York.
61. Gorenstein, D. G., Schroeder, S. A., Fu, J. M., Metz, J. T., Roongta, V., and Jones, C. R. (1988) *Biochemistry 27*, 7223−7237.
62. Altona, C. (1982) *Recl. Trav. Chim. Pays-Bas 101*, 413−433.
63. O'Brian, C. A. (1967) *Acta Crystallogr. 23*, 92−106.
64. Keniry, M. A. (2000) *Biopolymers 56*, 123−146.
65. Wang, Y., and Patel, D. J. (1994) *Structure 2*, 1141−1156.
66. Parkinson, G. N., Lee, M. P., and Neidle, S. (2002) *Nature 417*, 876−880.
67. Padmanabhan, K., Padmanabham, K. P., Ferrara, J. D., Sadler, J. E., and Tulinski, A. (1993) *J. Biol. Chem. 268*, 17651−17654.
68. Patel, P. K., and Hosur, R. V. (1999) *Nucleic Acids Res. 27*, 2457−2464.
69. Matsugami, A., Ouhashi, K., Kanagawa, M., Liu, H., Kanagawa, S., Uesugi, S., and Katahira, M. (2001) *J. Mol. Biol. 313*, 255−269.
70. Liu, H., Kugimiya, A., Sakurai, T., Katahira, M., and Uesugi, S. (2002) *Nucleosides, Nucleotides Nucleic Acids 21*, 785−801.
71. Kettani, A., Gorin, A., Majumdar, A., Hermann, T., Skripkin, E., Zhao, H., Jones, R., and Patel, D. J. (2000) *J. Mol. Biol. 297*, 627−644.
72. Kettani, A., Bouaziz, S., Skripkin, E., Majumdar, A., Wang, W. M., Jones, R. A., and Patel, D. J. (1999) *Struct. Folding Des. 7*, 803−815.
73. Miura, T., Benevides, J. M., and Thomas, G. J., Jr. (1995) *J. Mol. Biol. 248*, 233−238.
74. Sen, D., and Gilbert, W. (1990) *Nature 344*, 410−414.
75. Hansen, R. S., Canfield, T. K., Lamb, M. M., Gartler, S. M., and Laird, C. D. (1993) *Cell 73*, 1403−1409.
76. Gurunathan, S., Klinman, D. M., and Seder, R. A. (2000) *Annu. Rev. Immunol. 18*, 927−974.
77. Krieg, A. M. (2002) *Annu. Rev. Immunol. 20*, 709−760.
78. Kandimalla, S. A. E. R. (2002) *Trends Mol. Med. 8*, 114−121.

BI0355185